Nanoscale Properties and Matrix−Dopant Interactions in Dye-Doped Organically Modified Silicate Thin Films

Angela M. Bardo, Maryanne M. Collinson,* and Daniel A. Higgins*

Department of Chemistry, Kansas State University, Manhattan, Kansas 66506

Received April 12, 2001. Revised Manuscript Received June 7, 2001

The nanoscale properties of organically modified sol−gel-derived silicate thin films are studied in detail by single-molecule spectroscopic methods. For these studies, the solvent-sensitive probe Nile Red is doped into the films at nanomolar concentrations. Spectroscopic data are obtained for films prepared from sols containing different mole fractions of isobutyltrimethoxysilane and tetraethoxysilane. The data are analyzed using a model based on Marcus theory, providing important new information on static local film properties such as polarity and the extent of specific dopant−matrix interactions. Data on dynamic phenomena related to local matrix rigidity is also obtained. In general, throughout the range of samples studied, the most polar environments are also found to be the most rigid. With regard to their static properties, broad heterogeneous distributions are found in films of predominantly inorganic composition. In several instances, bimodal distributions are also observed, which result from specific chemical interactions and likely involve hydrogen bonding of the dye to the silicate matrix and/or to entrapped solvent. As the organic content of the film is increased, the film environments become less polar, less rigid, and more homogeneous. In addition, the effects of specific chemical interactions become dramatically less apparent. With respect to dynamic film properties, two distinct distributions are observed in films of intermediate organic/inorganic composition, reflecting the presence of environments differing in their rigidity. Studies of time-dependent single-molecule fluorescence fluctuations provide support for the conclusions derived from the spectroscopic data.

I. Introduction

Organically modified silicate (ORMOSIL) glasses are prepared by the hydrolysis and co-condensation of appropriate inorganic and organosilicon precursors.[1−4] Compared to materials produced from the individual components, ORMOSILs often have enhanced physicochemical properties.[1−4] These materials were first reported in the literature in the mid 1980s[5,6] and are now being developed for use in abrasion-resistant and functional coatings,[7−12] chemical sensors,[1] electro-optical[13,14] and photochromic materials,[15] optical waveguides,[16,17] tunable solid-state lasers,[18] and as stationary phases for chromatography.[19,20] For optimization of device performance, all such applications require a detailed understanding of their chemical and physical properties. As a result, extensive effort has been devoted to their characterization. Historically, such studies have utilized several different bulk techniques to understand average material properties such as polarity, hardness, porosity, and optical clarity.[21−26] Naturally, these attributes vary between materials prepared under different conditions and from different precursor sols. It is now understood that as the fraction of organosilicon precursor is increased, the average porosity and surface area of the matrix changes, leading to a decrease in matrix rigidity.[27] Such changes are expected because the organically

* To whom correspondence should be addressed. E-mails: mmc@ksu.edu; higgins@ksu.edu.

(1) Collinson, M. M. *Mikrochim. Acta* **1998**, *129*, 149.
(2) Avnir, D.; Klein, L. C.; Levy D.; Schubert, U.; Wojcik, A. B. *The Chemistry of Organic Silicon Compounds*, Vol. 2; Rappoport, Z., Apeloig, Y., Eds.; John Wiley & Sons: New York, 1998; p 2317.
(3) Wen, J.; Wilkes, G. L. *Chem. Mater.* **1996**, *8*, 1667.
(4) Schubert, U.; Hüsing, N.; Lorenz, A. *Chem. Mater.* **1995**, *7*, 2010.
(5) Schmidt, H. *Mater. Res. Soc. Symp. Proc.* **1984**, *32*, 327.
(6) Philipp, G.; Schmidt, H. *J. Non-Cryst. Solids* **1984**, *63*, 283.
(7) Schmidt, H. *J. Non-Cryst. Solids* **1985**, *73*, 681.
(8) Schmidt, H.; Rinn, G.; Nab, R.; Sporn, D. *Mater. Res. Soc. Symp. Proc.* **1988**, *121*, 743.
(9) Schmidt, H. *Mater. Res. Soc. Symp. Proc.* **1990**, *171*, 3.
(10) Schmidt, H.; Wolter, H. *J. Non-Cryst. Solids* **1990**, *121*, 428.
(11) Wen, J.; Vasudevan, V. J.; Wilkes, G. L. *J. Sol-Gel Sci. Technol.* **1995**, *5*, 115.
(12) Hsueh, C.; Collinson, M. M. *J. Electroanal. Chem.* **1997**, *420*, 243.
(13) Boilot, J.-P.; Biteau, J.; Brun, A.; Chaput, F.; Dantas de Morais, T.; Darracq, B.; Gacoin, T.; Lahlil, K.; Lehn, J.-M.; Levy, Y.; Malier, L.; Tsivgoulis, G.-M. *Mater. Res. Soc. Symp. Proc.* **1998**, *519*, 227.
(14) Levy, D.; Esquivias, L. *Adv. Mater.* **1995**, *7*, 120.
(15) Levy, D. *Chem. Mater.* **1997**, *9*, 2666.
(16) Sorek, Y.; Reisfeld, R.; Tenne, R. *Chem. Phys. Lett.* **1994**, *227*, 235.
(17) Yang, L.; Saavedra, S. S.; Armstrong, N. R.; Hayes, J. *Anal. Chem.* **1994**, *66*, 1254.
(18) Altman, J. C.; Stone, R. E.; Nishida, F.; Dunn, B. *Proc. SPIE* **1992**, *1758*, 507.
(19) Wang, D.; Chong, S. L.; Malik, A. *Anal. Chem.* **1997**, *69*, 4566.
(20) Guo, Y.; Colón, L. *Anal. Chem.* **1995**, *67*, 2511.
(21) Lobnik, A.; Wolfbeis, O. S. *Proc. SPIE* **1997**, *3136*, 284.
(22) Matsui, K.; Nozawa, K. *Bull. Chem. Soc. Jpn.* **1997**, *70*, 2331.
(23) Moreno, E. M.; Levy, D. *Chem. Mater.* **2000**, *12*, 2334.
(24) Dunn, B.; Zink, J. *J. Mater. Chem.* **1991**, *1*, 903.
(25) Pandey, S.; Baker, G. A.; Kane, M. A.; Bonagni, N. J.; Bright, F. V. *Chem. Mater.* **2000**, *12*, 3547.
(26) Dunn, B.; Zink, J. I. *Chem. Mater.* **1997**, *9*, 2280.
(27) Yan, Y.; Hoshino, Y.; Duan, Z.; Chaudhuri, S. R.; Sarkar, A. *Mater. Res. Soc. Symp. Proc.* **1996**, *435*, 307.

10.1021/cm010296n CCC: $20.00
Published on Web 07/10/2001

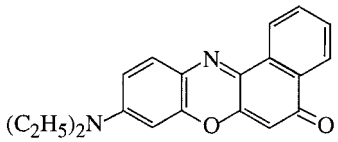

Figure 1. Chemical structure of Nile Red (NR).

functionalized precursors have fewer reactive (cross-linkable) sites and, hence, form a more open silicate network. Simultaneously with these structural changes, the average material polarity may either increase or decrease, depending on the chemical structures of the organosilicon precursors.

While average materials properties have been extensively studied, the physicochemical properties of the individual nanoscale environments found within individual films and/or monoliths are less well understood.[24−26] The properties of these environments can vary tremendously, depending on the local degree and/or rate of hydrolysis and condensation of each silicate precursor, possibly leading to the formation of domains with distinct chemical composition.[26] Such information is very difficult to extract from the results of bulk experiments.

Previously, we have utilized single-molecule spectroscopic (SMS) methods[28−30] to obtain insight into the nanoscale variations of sol−gel films formed from nonfunctionalized tetramethoxysilane and have made comparisons[28] with organic polymer films.[29] In these experiments, a much broader range of environments was found for the silicate samples. In other studies, we elucidated the effects of film drying conditions on local environmental properties.[30] The SM data obtained showed that environmental rigidity increased significantly with drying, dramatically reducing oxygen permeability and increasing dopant photochemical stability. In the present investigation, SMS methods are employed to characterize the nanoscale environments found in ORMOSIL films prepared from sols containing varying mole fractions of isobutyltrimethoxysilane (BTMOS) and tetraethoxysilane (TEOS). To uncover variations in environmental properties caused by changes in precursor composition, other variables such as humidity, drying time, and temperature are held approximately constant. The solvent-sensitive dye Nile Red (NR, Figure 1) is doped into the films at nanomolar levels and is used as a spectroscopic probe of the nanoscale environments.[29] Observed variations in local film properties result from nanoscale variations in material polarity and rigidity but also reflect variations in the occurrence of specific dopant−matrix interactions, such as hydrogen bonding. Time-dependent studies[30−33] of spectrally integrated NR emission are used to obtain complementary data and provide support for the conclusions drawn from the spectroscopic results.

(28) Wang, H.; Bardo, A. M.; Collinson, M. M.; Higgins, D. A. *J. Phys. Chem. B* **1998**, *102*, 7231.
(29) Hou. Y.; Bardo, A. M.; Martinez, C.; Higgins, D. A. *J. Phys. Chem. B* **2000**, *104*, 212.
(30) Mei, E.; Bardo, A. M.; Collinson, M. M.; Higgins, D. A. *J. Phys. Chem. B* **2000**, *104*, 9973.
(31) Yip, W.-T.; Hu, D.; Yu, J.; Vanden Bout, D. A.; Barbara, P. F. *J. Phys. Chem. A* **1998**, *102*, 7564.
(32) Weston, K. D.; Carson, P. J.; Metiu, H.; Buratto, S. K. *J. Chem. Phys.* **1998**, *109*, 7474.
(33) Dickson, R. M.; Cubitt, A. B.; Tsien, R. Y.; Moerner, W. E. *Nature* **1997**, *388*, 355.

II. Experimental Considerations

Sample Preparation. ORMOSIL films were prepared from tetraethoxysilane (TEOS, Aldrich, 99+%) and isobutyltrimethoxysilane (BTMOS, Fluka 95%). For each sol a 1:4:4.5:0.005 (total silicate:ethanol:water:0.1 M HCl) mixture was stirred for 30 min and allowed to age for approximately 48 h. Methanolic Nile Red (NR) solution was then added to the sol to give a final dye concentration of 0.5−1 nM. Immediately following the addition of the dye, the sol was spin-cast (6000 rpm) onto a clean glass microscope coverslip (Fisher), resulting in films of 350−550 nm in thickness. The films were then dried for 18−24 h at 30% humidity and room temperature. All SM experiments were performed at room temperature under ambient humidity in the 25−40% range. In some situations, a dry air purge was used to maintain low-humidity conditions. Bulk studies were performed on 3−5-μm thick films prepared by spin-casting multiple layers of 1-μM NR sol onto the same glass substrates. These films were dried and aged under conditions similar to those used for single-molecule samples. Samples prepared from sols ranging from 10 to 100 mol % BTMOS (relative to total silicate) were characterized. In all cases, TEOS comprised the remaining mole percentage. The film samples are classified below by the mole percent of BTMOS used in sol preparation. For example, a film prepared from a sol of 10:90 (BTMOS:TEOS) mole ratio is referred to as a "10% BTMOS" film, although the final films actually contain little or no residual BTMOS. Final film composition was confirmed by Fourier transform infrared (FTIR) spectroscopy studies[34,35] of films deposited on silicon wafers. As expected, the absorption bands for the C−H stretching and Si−CH_2− deformation modes (i.e., in the 2960−2860-cm^{-1} range and at 1230 cm^{-1})[34,35] in the films increased approximately linearly with BTMOS content in the precursor sol.

Instrumentation. The confocal microscope used in these experiments has been described previously.[28] Briefly, the 543-nm line from a helium−neon laser was used to excite the NR molecules. A dichroic beam splitter (Chroma Technologies) was used to direct the light into a 100X, 1.3 numerical aperture (NA) objective, which was used to produce a diffraction-limited focus of ≈300-nm diameter on the sample. The sample was mounted on a piezo-electric scanning stage (Queensgate) employing closed-loop X,Y feedback. This stage was in turn mounted to an inverted epi-illumination microscope (Nikon). Fluorescence from individual molecules was collected using the same 1.3 NA objective and was isolated from residual 543-nm light by the dichroic beam splitter and appropriate notch and band-pass filters (passing light to the red of 17 500 cm^{-1}). Individual molecules were located by recording fluorescence images of 5-μm square sample regions. A single-photon counting avalanche diode (EG&G Canada) was used to detect single-molecule fluorescence in imaging and time-dependent experiments. The fluorescence signal was integrated for 40 ms/pixel in the 100 × 100 pixel images. In time-dependent experiments, the spectrally integrated fluorescence from each sample region (nominally from a single molecule) was collected with 10-ms resolution. Fluorescence spectra were collected using an imaging spectrograph and liquid-nitrogen-cooled CCD array (Roper Scientific). Bulk fluorescence spectra were taken using a commercial fluorometer (Spex Fluoromax).

III. Results and Discussion

Imaging. Figure 2 presents typical fluorescence images of 5-μm square regions recorded for films prepared with different fractions of organic and inorganic precursors. Such images were recorded primarily for the purpose of locating single molecules for spectral and temporal analysis (see below). However, they also give initial, qualitative information on film properties.

(34) Almeida, R. M.; Pantano, C. G. *J. Appl. Phys.* **1990**, *68*, 4225.
(35) Yang, L.; Saavedra, S. S.; Armstrong, N. R. *Anal. Chem.* **1996**, *68*, 1834.

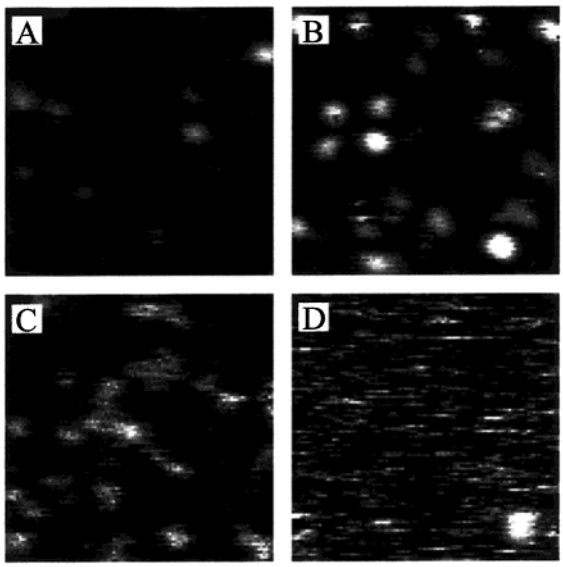

Figure 2. Fluorescence images of silicate thin films containing single NR molecules. The films were prepared from sols containing (A) 10%, (B) 33%, (C) 66%, and (D) 100% BTMOS. Dramatically increased signal fluctuations are exhibited in films of higher organic content.

The images of films with low organic content show bright round fluorescent spots of diffraction limited size. With the aid of additional evidence (i.e., fluorescent spot number density, emission rate, and blinking and photobleaching behavior),[28,36] it may be concluded that the bright spots represent fluorescence from single molecules. As the organic content of the film is increased, two trends are observed in the images. First, the apparent number density of fluorescent spots increases, suggestive of an increase in the number density of fluorescent single molecules. Because all samples were prepared with similar concentrations of NR, the apparent increase in density of molecules is likely due to an increase in fluorescence excitation and/or emission efficiency (e.g., quantum yield) as the polarity of the matrix is reduced. Indeed, bulk solution-phase studies of NR show an increase in the fluorescence quantum yield with decreasing solvent polarity.[37,38] For example, the quantum yield of NR in methanol has been measured to be 0.08, while in chloroform a value of 0.33 was obtained.[37]

Second, with increasing organic content, the images take on a "streaky" appearance and the molecules no longer appear as full, round spots. The streaks are not noise, having signal levels significantly greater than the background and similar to the full, round spots observed in other samples. Instead, they arise from temporal variations in the single-molecule emission rate that occur on time scales similar to that of a single line scan. The apparent increase in the rate of signal fluctuations manifested by these streaks suggests that more fluid-like, dynamic, nanoscale environments are formed in films of greater organic content. The signal fluctuations likely arise from phenomena such as translational[39,40] and rotation diffusion,[41,42] spectral diffusion,[43−45] and/or variations in the quantum yield.[29,37,38] A long-lived triplet state may also contribute to variations in the fluctuation rate.[31−33,46] The exact origins of these fluctuations are currently being investigated, as discussed further below.

Spectral Studies. As is now well-known,[47] the NR fluorescence spectrum is highly sensitive to the exact nature of the surrounding solvent environment. Indeed, we have previously employed NR as a probe of environmental polarity in single-molecule studies of organic polymer films.[29] In the present work, the emission spectra of NR single molecules are used in a similar manner. Spectra were recorded for approximately 200 single molecules in each ORMOSIL film. Only spectra from single molecules that clearly remained in fixed locations during imaging were employed. As a result, only films prepared from sols containing 10−75% BTMOS were characterized (referred to below as "10−75% BTMOS" samples). Data from 0% BTMOS samples were not employed because they did not accurately reflect the spectral distributions observed in bulk samples (see below). Each SM spectrum was fit with two Gaussian functions. Inclusion of the second Gaussian allowed for the spectra to be properly fit in the presence of a vibronic sideband of variable intensity and position. The emission maximum (ν_{fl}) and full-width at half-maximum (fwhm, $\delta\nu_{fl}$) of the spectrum were taken from the fitting parameters for the peak centered at higher energy.

Histograms (not shown here) of ν_{fl} and $\delta\nu_{fl}$, prepared from the above single-molecule data, were also fit with Gaussian functions to obtain qualitative measures of average film properties. The ν_{fl} distribution averages and ν_{fl} distribution widths (fwhm) were determined from these fits and are reported in Table 1, as are the related parameters for the $\delta\nu_{fl}$ distributions. Note that the fwhm of each distribution reflects the degree of sample heterogeneity. In some cases a bimodal distribution was observed, these histograms were fit with a pair of Gaussians, and two values for each distribution average and width are reported.

Substantial information on local sample heterogeneity as a function of film composition can be obtained from the SM spectral data. To this end, the emission maxima (ν_{fl}) and emission bandwidths ($\delta\nu_{fl}$) for the individual molecules were analyzed using a modified form of Marcus theory for charge-transfer spectra.[48−53] This

(36) Betzig, E.; Chichester, R. J. *Science* **1993**, *262*, 1422.
(37) Dutta, A. K.; Kamada, K.; Koji, O. *J. Photochem. Photobiol. A: Chem.* **1996**, *93*, 57. The quantum yields were determined with respect to that of rhodamine 6G in ethanol.
(38) Sarkar, N.; Das, K.; Nath, D. N.; Bhattacharyya, K. *Langmuir* **1994**, *10*, 326.
(39) Schmidt, T.; Schütz, G. J.; Baumgartner, W.; Gruber, H. J.; Schindler, H. *J. Phys. Chem.* **1995**, *99*, 17662.
(40) Wirth, M. J.; Swinton, D. J. *J. Phys. Chem. B* **2001**, *105*, 1472.
(41) Deschenes, L. A.; Vanden Bout, D. A. *Science* **2001**, *292*, 255.
(42) Ha, T.; Enderle, T.; Chemla, D. S.; Selvin, P. R.; Weiss, S. *Phys. Rev. Lett.* **1996**, *77*, 3979.
(43) Lu, H. P.; Xie, X. S. *Nature* **1997**, *385*, 143.
(44) Ambrose, W. P.; Moerner, W. E. *Nature* **1991**, *349*, 225.
(45) Xie, X. S.; Dunn, R. C. *Science* **1994**, *265*, 361.
(46) Vanden Bout, D. A.; Yip, W.-T.; Hi, D.; Fu, D.-K.; Swager, T. M.; Barbara, P. F. *Science* **1997**, *277*, 1074.
(47) Deye, J. F.; Berger, T. A.; Anderson, A. G. *Anal. Chem.* **1990**, *62*, 615.
(48) Chen, P.; Meyer, T. J. *Chem. Rev.* **1998**, *98*, 1439.
(49) Lakowicz, J. R. *Principles of Fluorescence Spectroscopy*; Plenum: New York, 1983.
(50) Marcus, R. A. *J. Chem. Phys.* **1965**, *43*, 1261.
(51) Marcus, R. A. *J. Phys. Chem.* **1989**, *93*, 3078.
(52) Marcus, R. A. *J. Phys. Chem.* **1990**, *94*, 4963.
(53) Brunschwig, B. S.; Ehrenson, S.; Sutin, N. *J. Phys. Chem.* **1987**, *91*, 4714.

Table 1. Average Spectroscopic Parameters Obtained by Fitting the Histograms of the Single-Molecule Data to Gaussian Functions[a]

BTMOS	10%	25%	33%	50%	66%	75%
ν_{fl} average (±20)	16 420, 17 280[b]	16 550	16 500	16 580	16 710	16 610
ν_{fl} fwhm (±30)	890, 200[b]	730	700	500	370	180
$\delta\nu_{fl}$ average (±20)	810	1090	920	860, 1320	1340	1400
$\delta\nu_{fl}$ fwhm (±20)	680	870	730	360, 300	280	370

[a] Average values (peak maximum) and distribution widths (fwhm) for ν_{fl} and $\delta\nu_{fl}$ from these histograms are shown. The values in parentheses represent the average error. All values are in cm^{-1}. [b] Possibly truncated due to optical filters.

theory, relevant for partially "frozen" environments in solid materials,[52] has been described previously in detail.[29] Briefly, the free energy change for the electronic transition, $\Delta\Delta G°$, relative to that in a vacuum, $\Delta G_v°$, is determined, as is the total reorganization energy, λ, associated with the residual (unfrozen) motions of the matrix and dye. These parameters are related to the spectroscopic parameters as follows:

$$\nu_{fl} = \Delta G_v° - \Delta\Delta G° - \lambda \quad (1)$$

$$\delta\nu_{fl} = 4(\lambda(\ln 2)kT)^{1/2} \quad (2)$$

where k is the Boltzman constant and T is temperature. The value for $\Delta G_v°$ has previously been estimated to be 20 600 cm^{-1} from bulk solution phase spectroscopic studies.[29] The above equation for $\delta\nu_{fl}$ is derived in a classical fashion and describes the fwhm of a single vibronic band broadened by low-frequency motions of the molecule and matrix.

In the interpretation of $\Delta\Delta G°$ and λ, it is usually assumed that the local solvent environment behaves as a dielectric continuum that may be described by its static and optical dielectric constants (ϵ and η^2). Here, $\Delta\Delta G°$ is interpreted as a more general spectroscopic parameter that describes not only the local polarity but also includes additional contributions from any specific chemical interactions (i.e., hydrogen bonding) between the matrix or residual solvent and the fluorescent dye. It also includes contributions resulting from the "freezing" of matrix dipole motions in these solid samples.[52] The value of $\Delta\Delta G°$ then describes the "static" transition energy after all relaxation processes have ceased.

The value of λ is associated with dynamic motions of the surrounding matrix dipoles and/or dynamic changes in the dye molecule itself that occur during the excited-state lifetime.[54] Again, for solid samples, λ actually describes the residual "unfrozen" matrix and molecular motions.[52] An increase in molecular and/or environmental mobility results in a larger λ value. Specific chemical interactions only alter its value if the nanoscale dynamics are changed by these interactions. Finally, it should be noted that spectral diffusion on a time scale shorter than that used to record the SM fluorescence spectra, but longer than the fluorescence lifetime, contributes to the observed spectral widths. As a result, erroneously large λ values may be obtained. However, all such spectral dynamics also reflect environmental fluidity and therefore do not alter the conclusions drawn below from the measured λ values.

Figure 3 presents histograms of the $\Delta\Delta G°$ and λ values obtained from the SM data. As can be seen from these data, the $\Delta\Delta G°$ and λ distribution widths change

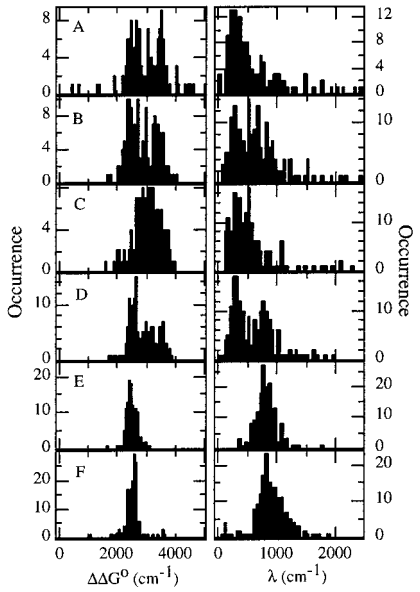

Figure 3. Histograms of the transition energy, $\Delta\Delta G°$ (left), and reorganization energy, λ (right), for NR calculated from SM spectroscopic data. Data from (A) 10%, (B) 25%, (C) 33%, (D) 50%, (E) 66%, and (F) 75% BTMOS samples.

dramatically with increased film organic content. Broad distributions in $\Delta\Delta G°$ are found in films of low organic content, reflecting the broad distribution of nanoscale environments present in these films. In the films of lowest organic content, the broad $\Delta\Delta G°$ distributions appear to be comprised of two distinct distributions. This result suggests film heterogeneity arises from the presence of (at least) two distinct classes of nanoscale environments in these samples. Each of these appears to be relatively homogeneous, having widths similar to those found in films of higher organic content. Interestingly, the distribution centered at larger $\Delta\Delta G°$ values disappears in samples of greater than 50% BTMOS. As a result, the total widths of the $\Delta\Delta G°$ histograms are found to be substantially narrower for films of greater organic content. The latter observation indicates that the nanoscale environments within the films become more homogeneous with respect to static polarity and matrix interactions as the organic content of the film increases.

The widths of the λ histograms are similar and relatively narrow in samples of both high and low fractions of BTMOS. This indicates that the dynamic properties are relatively homogeneous for these films. For films of intermediate composition, two distinct distributions are observed (Figure 3). These two distributions suggest there are two classes of local film rigidity. The extent to which each distribution appears is strongly dependent on the composition (BTMOS mole percent) of the sol used for film preparation.

(54) Krishna, M. M. G. *J. Phys. Chem. A* **1999**, *103*, 3589.

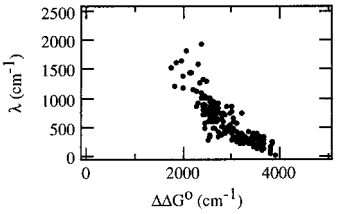

Figure 4. Plot of λ vs $\Delta\Delta G°$ for 50% BTMOS films. The data show the existence of two distributions in both parameters. Also shown is the overall negative correlation between these sets of data, indicating the more rigid nanoscale environments are also more polar.

The average (peak) values of the $\Delta\Delta G°$ and λ histograms also show dramatic variations as organic functionality is incorporated into the films. Samples of high organic content have a small average value of $\Delta\Delta G°$, reflecting the relatively nonpolar environments that are expected for these materials. For films of low organic content, the distribution shifts to larger values on average, indicative of the more polar environments found in these films. Again, this shift to larger values results from the appearance of the second distribution centered at large $\Delta\Delta G°$ values for films of low organic content. The distribution centered at small $\Delta\Delta G°$ values appears to remain at the same position in all the samples. Similarly, the distribution at large $\Delta\Delta G°$ values also seems to remain in a fixed location. These results suggest that the two distinct classes of environment found in films of low organic content differ in their static properties. The two distributions then reflect the presence of environments differing in static polarity or in the types of chemical interactions that occur between the matrix and dye molecules.

Along with the above variations in static local film properties, the average fluidity of the sample also changes with film composition, as indicated by the histograms in Figure 3. It is particularly noteworthy that the λ distributions appear to shift discretely from large values to small values as the organic content of the film decreases. This discrete change in apparent environmental fluidity occurs in films of approximately 50% BTMOS.

Interestingly, the 50% BTMOS samples show strong evidence of bimodal distributions in both $\Delta\Delta G°$ and λ histograms. Possible correlations between these two parameters were investigated by plotting λ versus $\Delta\Delta G°$ for each molecule. Figure 4 shows such a plot for the 50% BTMOS samples. It is clearly indicated in this plot (and in those from other samples) that molecules with high $\Delta\Delta G°$ values have relatively low λ values and vice versa. It may then be concluded that, in general, the more polar nanoscale environments are more rigid. It is also apparent from Figure 4 that the $\Delta\Delta G°$ and λ values tend to "cluster" around certain regions. The results further support the above conclusions that the bimodal $\Delta\Delta G°$ and λ distributions reflect the presence of distinct classes of nanoscale environments in these materials. These phenomena are discussed further, below.

Possible origins for the observed variations in environmental properties are suggested by the chemical nature of the precursors used in film formation. Samples with low organic content have more highly constricted environments due to substitution of the trifunctional silicon alkoxide (BTMOS) with the tetrafunctional species (TEOS). Furthermore, because these films have greater cross-link density, matrix rigidity is also increased relative to films of higher organic content. This phenomenon is directly evidenced by the smaller λ values found in films of low organic content. Furthermore, because these films were prepared from sols of larger mole fractions of TEOS, the concentration of surface hydroxide species may be larger and more variable. As a result, the distributions of nanoscale properties become more inhomogeneous, as reflected in the relatively broader, bimodal $\Delta\Delta G°$ histograms.

Some of the observed heterogeneity in these samples may result from variable hydrogen bonding between the dye and other solvent and/or matrix molecules. For the constricted environments in samples of low organic content, the dye molecules are likely to be forced into close proximity to the surface hydroxide groups within the sol−gel matrix.[55] In addition, they may also interact more strongly with residual water in the film. Hydrogen bond formation to NR (see Figure 1) results in appreciable changes in the NR absorption and emission spectra. Charge transfer to the NR carbonyl group (the primary hydrogen-bond acceptor) following excitation is enhanced by hydrogen bonding, causing a red shift in its absorption and emission spectra. The shift in emission maximum appears as a larger value of $\Delta\Delta G°$ in the SM results. The distribution occurring at larger $\Delta\Delta G°$ values in Figure 3 for the samples of low organic content is qualitatively consistent with the presence of hydrogen-bound NR molecules. The distribution centered about smaller $\Delta\Delta G°$ values is likely due to "free" NR confined in constrained environments having lower concentrations of available surface hydroxide groups.

The addition of trifunctional BTMOS to the precursor sol significantly lowers the extent of cross-linking and reduces the surface hydroxide concentration in the films. This is reflected in the histograms of $\Delta\Delta G°$ and λ for samples of high organic content. Large λ values and small $\Delta\Delta G°$ values point to more fluid, less polar environments. With increased film porosity, the NR molecules are no longer restricted to near-surface regions, reducing the extent of hydrogen bonding, regardless of surface hydroxide concentration. As a result of these phenomena, a single, narrow $\Delta\Delta G°$ distribution is observed for films of high organic content, reflecting increased material homogeneity.

Bulk solution phase spectroscopy was used to obtain the approximate spectral shift expected between hydrogen-bound and "free" NR. Because the emission maximum and $\Delta\Delta G°$ are directly related, an identical shift in $\Delta\Delta G°$ is expected if hydrogen bonding to the dye does not alter the molecular and/or matrix reorganization energies. Acetonitrile and methanol were chosen for this study. Between these two solvents, the bulk NR absorption and emission spectra are shifted by about 610 and 640 cm^{-1}, respectively, as shown in Figure 5. Because acetonitrile cannot hydrogen bond to NR and because the two solvents have similar dielectric constants (35.95 and 32.66)[56] and similar orientation polarizabilities (0.305 and 0.309),[56] virtually the entire red shift ob-

(55) Rivera, D.; Harris, J. M. *Anal. Chem.* **2001**, *73*, 411.
(56) Reichardt, C. *Solvent and Solvent Effects in Organic Chemistry*; VCH: New York, 1988.

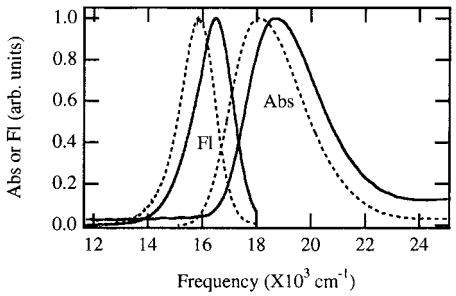

Figure 5. Bulk absorption and fluorescence spectra of NR in acetonitrile (—) and methanol (- - -), showing the dependence of the spectra on hydrogen bonding between dye and solvent.

served in methanol is attributable to hydrogen-bonding interactions with the solvent. Furthermore, because the Stokes shifts between the absorption and emission maxima in each solvent are very similar, hydrogen bonding is concluded to have little effect on the value of λ.

The two peaks in the $\Delta\Delta G°$ distribution obtained from the SM results for films of low organic content are separated by about 870 cm^{-1} (see Figure 3). The similarities in the spectral shifts for the bulk solvents and SM data lend support to the conclusion that the bimodal distribution in $\Delta\Delta G°$ likely reflects the presence of both "free" and hydrogen-bound NR. Again, hydrogen bonding may occur between the dye and matrix or the dye and entrapped solvent.

The behavior of the bimodal distributions in the $\Delta\Delta G°$ histograms as film organic content is increased supports the conclusion that the two distributions arise from discrete differences in the nanoscale properties. Importantly, the two distributions do not simply shift and merge in a continuous fashion. Rather, the number density of the more polar sites changes with film composition while their properties remain approximately constant. Such observations are consistent with the hydrogen-bonding mechanism described above. Were the two environments formed from continuously variable mixtures of the two precursors, their properties would change gradually with the composition of the initial sol.

It is also possible that the bimodal distribution in $\Delta\Delta G°$ is due to phase separation[57−59] of rigid environments of low organic content and fluid environments of high organic content. However, the single distribution in λ for films of low organic content (i.e., 10% BTMOS) indicates the two $\Delta\Delta G°$ distributions have similar rigidity. As a result, it is unlikely their appearance arises from phase separation. In this event, a bimodal distribution would be expected in the corresponding λ histograms. The observation of a single λ distribution again points to the likely importance of hydrogen bonding in the spectroscopic data. As noted above, little or no effect on λ is expected for such interactions.

Finally, it should be noted that all sample environments probed by the dye appear to be faithfully reflected

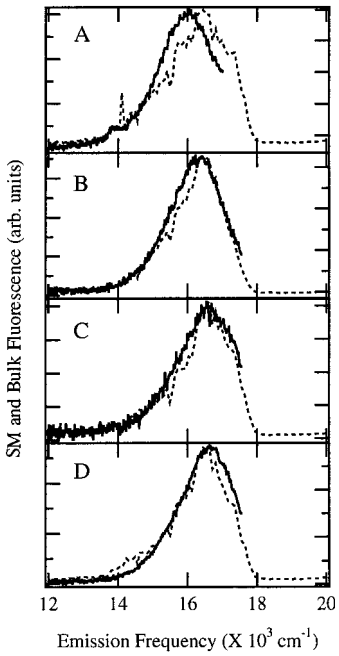

Figure 6. Overlay of summed SM (- - -) and bulk spectra (—) for NR in (A) 10%, (B) 33%, (C) 66%, and (D) 75% BTMOS films. The plots show the SM results faithfully represent the entire distribution of environments probed. The optical filters employed in the SM experiments block light to the blue of 17500 cm^{-1}.

in the SM fluorescence data. To test this hypothesis, bulk fluorescence spectra of NR in 3−5-μm thick films were recorded and compared to simulated "bulk" data obtained by summing the individual SM spectra. Four sets of these spectra are shown in Figure 6. The summed SM spectra compare very well with the bulk spectra in most cases. Therefore, it may be concluded that the models presented above represent a relatively complete picture of the nanoscale environments probed in these samples. Notable exceptions do, however, exist. For example, in the films of lowest organic content (Figure 6A), the bulk spectra are significantly red-shifted from the SM data. The discrepancy between the spectra was greatest for 0% BTMOS films, which, as a result, were not employed in the single-molecule spectral analysis. The poor overlap between these spectra is likely due to the limitations of SM methods when extremely solvent-sensitive dyes are employed. Molecules in the most polar environments are less efficiently excited by the 543-nm light employed. Furthermore, because the fluorescence quantum yield of NR is relatively small in polar environments, its emission is further weakened. As a result, molecules in the most polar environments (i.e., molecules that emit furthest to the red) appear as weaker fluorescent spots in the images and are selected less often for spectroscopic interrogation. Although problematic, such effects do not alter the above conclusions about the nature and origins of film heterogeneity. Although it is not possible to deduce exactly where these "missing" molecules would fall in the distributions shown in Figure 3, it is likely they would reflect the presence of environments of either much greater polarity or fluidity. Because of the trend toward greater polarity and rigidity observed for films of lower organic content, it is believed the missing molecules would simply lead to a further broadening of the $\Delta\Delta G°$

(57) Jiménez-Riobóo, R. J.; García-Hernández, M.; Prieto, C.; Fuentes-Gallego, J. J.; Blanco, E.; Ramírez-del-Solar, M. *J. Appl. Phys.* **1997**, *81*, 7739.
(58) Fyfe, C. A.; Aroca, P. P. *J. Phys. Chem. B* **1997**, *101*, 9504.
(59) Blanco, E.; García-Hernández, M.; Jiménez-Riobóo, R. J.; Litrán, R.; Prieto, C.; Ramírez-del-Solar, M. *J. Sol-Gel Sci. Technol.* **1998**, *13*, 451.

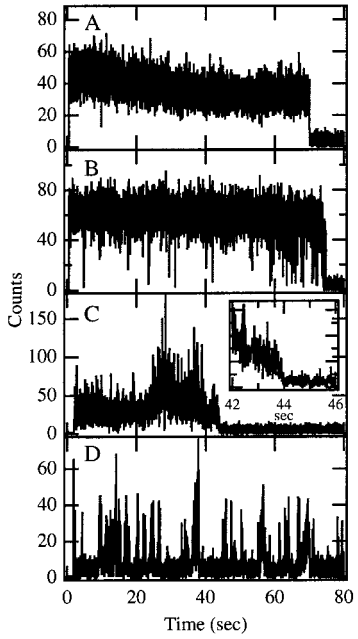

Figure 7. Single-molecule fluorescence transients for NR in (A) 10%, (B) 33%, (C) 66%, and (D) 100% BTMOS films. The increased signal fluctuations observed in films of intermediate−high organic content are attributed to increased fluctuations in the SM fluorescence quantum yield and molecular diffusion. The inset in (C) shows the gradual decay of the signal, rather than a discrete bleaching transition, consistent with a slow change in its photophysical properties and/or diffusion of the molecule out of the focal region.

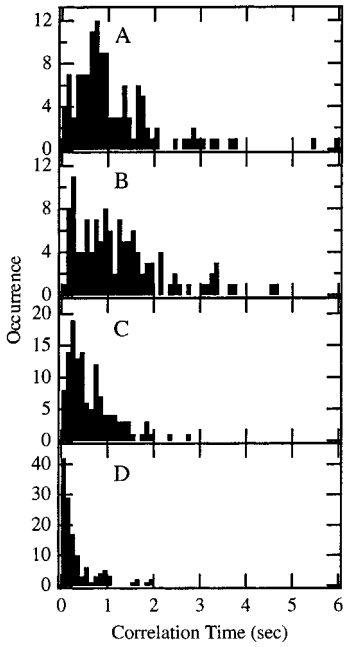

Figure 8. Histograms of signal correlation times calculated from autocorrelation of the SM fluorescence transients for NR in (A) 10%, (B) 33%, (C) 66%, and (D) 100% BTMOS films. The average correlation times for these samples were found to be 1.1, 1.3, 0.6, and 0.3 s (all ±0.2 s), respectively.

distributions toward greater polarity. Therefore, the films of low BTMOS content are likely even more heterogeneous than the data in Figure 3 suggests.

It is particularly important that the bulk spectra presented in Figure 6 exhibit very few differences across the entire range of ORMOSIL samples studied. Their widths are all large and similar. Only a slight blue shift in the bulk emission maximum with increasing film organic content is observed as well. While the bulk spectra incorporate information on sample heterogeneity, the exact origins of the spectral shifts and peak broadening are ambiguous. It is clear the SM data provide much more detailed information on nanoscale film properties. The broad distributions for $\Delta\Delta G°$ in samples of low organic content indicate static sample heterogeneity is relatively important in determining the widths of the bulk spectra. As the fraction of BTMOS is increased, dynamic solvation effects (signified by larger λ values) become more important. Finally, the bifurcation of the $\Delta\Delta G°$ and λ distributions are entirely obscured in the bulk analysis, masking the possible effects of hydrogen bonding.

Time-Dependent Analysis. The rate and extent of fluctuations observed in the spectrally integrated single-molecule emission also provides information on nanoscale film properties. Figure 7 shows examples of the transients obtained as a function of film organic content. In these transients, the streaks seen in the images (Figure 2) are manifested as signal fluctuations that occur on a time scale longer than the time resolution of the experiment (10 ms). Clearly, the signal fluctuations observed are highly dependent on film composition. As stated above, these signal fluctuations have several possible origins. Included are triplet blinking,[31−33,46] variations in the excitation efficiency due to spectral diffusion,[43−45] and time-dependent variations in the fluorescence quantum yield.[29,37,38] Physical processes such as translational and rotational molecular motions may also contribute.[39−42] With the possible exception of triplet blinking, the vast majority of causes for the signal fluctuations are related to environmental and/or dye molecule dynamics. Therefore, the signal transients provide an additional, complementary means of monitoring the fluidity of individual nanoscale environments.

A quantitative measure of the extent of signal fluctuations observed for each molecule was obtained by calculating the autocorrelation function for each transient. Previous publications have described the calculation and interpretation of autocorrelation data in detail.[30−33] For stochastic fluctuations, the autocorrelation function decays exponentially to zero. Exponential fitting of the decay yields the average signal correlation time. For NR, fluctuations are observed on two distinct time scales (milliseconds and seconds).[60] Therefore, the autocorrelations were fit with two exponentials. Only the first 10% of each autocorrelation was fit to avoid errors associated with the inclusion of statistically insignificant long time scale fluctuations. The first point in each was also excluded to avoid errors due to the effects of very rapid fluctuations and those due to shot noise. As the shorter time scale (ms) fluctuations likely include substantial contributions from triplet blinking,[31−33,46,60] only data on the longer time scale fluctuations are discussed here. Histograms of the SM signal correlation times obtained are shown in Figure 8 for a series of ORMOSIL samples. Each of the histograms contains data from approximately 100 transients. These histograms conclusively prove that the signal fluctuation rate increases with increasing film organic content.

(60) Hou, Y.; Bardo, A. M.; Higgins, D. A., unpublished results.

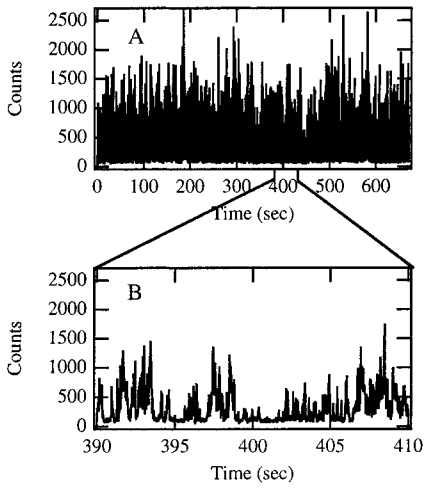

Figure 9. (A) High-power fluorescence transient of diffusing NR molecules in a 100% BTMOS film. (B) Expanded section of the transient in (A) showing the signal fluctuations more clearly. No clear photobleaching transition is observed for most transients in these samples, indicating single molecules are likely diffusing in and out of the microscope focus.

The lack of a clear trend in the data for low BTMOS percentage films (see Figure 8) has two possible origins. First, as the histograms broaden for the low BTMOS samples, the signal-to-noise for each histogram element becomes smaller and the trends between samples less apparent. Second, it is very likely more than one mechanism contributes to the signal fluctuations on these time scales. As the extent to which each mechanism contributes to the fluctuations and the characteristic time scale of these fluctuations are likely dependent on film composition, the trend may be complicated and even nonmonotonic. It is believed this latter effect is important here. In films of low organic content, one mechanism dominates and the data for 10 and 33% BTMOS show similar average correlation times. As the BTMOS percentage increases, one (or more) new mechanisms leading to faster fluctuations become important and shorter average correlation times are observed.

A closer look at Figure 7 gives qualitative information on the origins of the fluctuations in each sample. The SM fluorescence is nearly constant in Figure 7A (a typical transient for 10% BTMOS films), with the exception of shot noise. After approximately 70 s, this molecule photobleached in a discrete transition. In films of higher organic content, the molecules usually exhibit transitions to a "dark" or weakly emitting state that increases in lifetime with increasing film organic content. Figure 7B,C shows examples of these data (for 33 and 66% BTMOS samples). At the end of the transient in Figure 7C, the final drop in the signal to the background level is "gradual" and therefore does not appear to be due to photobleaching. Rather, it is likely the molecule has slowly diffused out of the microscope focus. The molecule may also have rotated or undergone a slow change in its photophysical properties. For 100% BTMOS samples (Figure 7D), the signal fluctuates rapidly in time, but surprisingly, no clear photobleaching transition is ever observed. Most molecules in these samples behave in a similar fashion, even at very high incident powers (see Figure 9). Again, the fluctuations observed on these longer time scales are not likely due to the formation of a "dark" triplet state. The triplet lifetime for NR has been measured to be ≈1 ms in other solid films.[60] The signal in these samples remains at the background level for seconds in the present experiments. Furthermore, because oxygen (an efficient triplet quencher) diffusion is known to become more rapid in organically modified silicate films,[61] the triplet lifetime is expected to decrease, rather than increase, with increasing film organic content. The behavior observed in 100% BTMOS films is then consistent with rapid translational diffusion of single molecules in and out of the microscope focus.[40] Indeed, wide-field illumination studies[39] show the molecules diffuse over several hundred nanometers on a 2-s time scale in these samples.[60] Unfortunately, it is difficult to determine the exact nature of the fluctuations in all of the samples.

Because of uncertainties in the origins of these fluctuations, and because of the associated difficulties in "locating" single molecules in images of the 100% BTMOS samples, the spectroscopic data obtained were not employed in the SM spectral analysis presented above. For all other samples (i.e., with BTMOS content less than or equal to 75%), signal fluctuations (due to translational diffusion and all other mechanisms) were far less prevalent. Stationary fluorescent "spots" attributable to SM emission could be located and their spectra recorded. In all cases, diffusing molecules were readily discriminated against by only taking spectra from single molecules that appeared to remain in a fixed location during imaging.

Other phenomena that may contribute to the observed signal fluctuations include rotational diffusion of the NR molecules. Indeed, fluorescence transients recorded for orthogonal emission polarizations[41] (reporting on in-plane SM rotations) often show the molecules rotating on the time scales of the observed fluctuations for samples of low and intermediate organic content. However, it is clear from picosecond-resolved fluorescence anisotropy studies of NR[62] in bulk ORMOSIL films that many molecules in the films of highest organic content rotate on pico-/nanosecond time scales.[60] These results are consistent with those obtained previously for other dyes in sol−gel-derived glasses.[63] Such fast motions would not contribute to the signal fluctuations.

The observed signal fluctuations may also reflect time-dependent variations in the fluorescence quantum yield. Indeed, the fluorescence quantum yield of NR is known to be highly sensitive to its environment.[29,37,38] This solvent sensitivity results primarily from the formation of a nonfluorescent twisted internal charge transfer (TICT) state in polar media.[37,38,64] Formation of the TICT state involves rotation of the diethylamine group from a planar orientation to one perpendicular to the NR ring structure. Variations in the quantum yield resulting from variations in the rate of crossing to and/or from the TICT state could then cause the observed fluctuations. Similar fluctuations would also occur if the properties of the nanoscale environment

(61) Liu, H.-Y.; Switalski, S. C.; Coltrain, B. K.; Merkel, P. B. *Appl. Spectrosc.* **1992**, *46*, 1266.
(62) Choi, M.; Jin, D.; Kim, H.; Kang, T. J.; Jeoung, S. C.; Kim, D. *J. Phys. Chem. B* **1997**, *101*, 8092.
(63) Narang, U.; Wang, R.; Prasad, P. N.; Bright, F. V. *J. Phys. Chem.* **1994**, *98*, 17.
(64) Datta, A.; Mandal, D.; Pal, S. K.; Bhattacharyya, K. *J. Phys. Chem. B* **1997**, *101*, 10221.

around each molecule fluctuate on a millisecond−second time scale.

While the signal fluctuations could arise from any of the above mechanisms (translational, rotational, or spectral diffusion, or variations in the fluorescence quantum yield), it is most significant that the rate of signal fluctuations are clearly related to film composition. Films of greatest organic content show the most substantial millisecond−second time scale fluctuations. As all the proposed mechanisms involve some type of dye and/or environmental motions, molecules exhibiting greater signal fluctuations most certainly are entrapped in more dynamic environments. As a result, it may be concluded that films of highest organic content incorporate the most dynamic nanoscale environments. Analogously, films of lowest organic content are comprised of primarily static, yet highly heterogeneous environments, as reflected by the broad distributions in the time scales for SM signal fluctuations in these samples. Future studies will focus more directly on the possible correlations between spectral and temporal data suggested by these results.

IV. Conclusions

Thin sol−gel films prepared from sols containing different mole fractions of inorganic and organically modified silicate precursors have been studied using SM spectroscopic methods. The data obtained have yielded valuable new information on the heterogeneity and nanoscale properties of these materials. Such information was shown to be obscured in bulk spectroscopic studies of these same samples. Local polarity, dye−matrix interactions (i.e., hydrogen bonding), and local environmental rigidity were explored. The observation of highly confined, rigid environments in films of low organic content is of relevance to sol−gel applications in solid-state optical systems. In such materials, it is desirable that the dopant molecules be permanently entrapped in environments that also protect them from reactive species (i.e., oxygen). For sensor and catalyst applications, it is desirable that the film environments be more fluid in nature, allowing sufficient dopant mobility so that proper reaction geometries can be achieved. The greater fluidity of the environments found in films of high organic content verifies that these materials are best suited for such applications. Finally, the results obtained indicate that films prepared from different organic−inorganic precursor mixtures do not lead to a continuous variation in film properties. Rather, discrete changes in film polarity, extent of specific dopant−matrix interactions, and environmental rigidity occur. These results point to the heterogeneous nature of ORMOSIL films; they also provide clear evidence as to the chemical origins of this heterogeneity.

Acknowledgment. The authors would like to thank Yanwen Hou, Ginagunta Saroja, and Rachel Allenbaugh for their contributions to this work. Funding was provided by the Army Research Office (DEPSCoR) and Kansas State University. A.M.B. and D.A.H. thank 3M Corporation for additional funding.

CM010296N